Two-Stage Aggregate Formation via Streams in Myxobacteria

M. S. Alber,[1], M. A. Kiskowski,[1], and Y. Jiang[2]
[1] *Mathematics and Physics Departments, University of Notre Dame, Notre Dame, IN 46556.*
[2] *Theoretical Division, Los Alamos National Laboratory, Los Alamos, NM 87545.*
(Dated: November 20, 2003)

In response to adverse conditions, myxobacteria form aggregates which develop into fruiting bodies. We model myxobacteria aggregation with a lattice cell model based entirely on short range (non-chemotactic) cell-cell interactions. Local rules result in a two-stage process of aggregation mediated by transient streams. Aggregates resemble those observed in experiment and are stable against even very large perturbations. Noise in individual cell behavior increase the effects of streams and result in larger, more stable aggregates.

PACS numbers: 87.18Ed, 05.65.+b, 87.18.Hf, 05.40.Ca

Introduction.— Fruiting body formation in bacteria occurs in response to adverse conditions [1] and is critical for species survival. To form fruiting bodies, many cells must first aggregate. Complex, multi-stage morphogenesis must be robust despite internal and external noise.

Canonically, models for bacteria (e.g. *E. Coli* [2, 3] and *Bacillus subtilis* [4, 5]) and amoebae (e.g. *Dictyostelium discoideum* [5, 6]) aggregation have been based on attractive chemotaxis, a long range cell interaction that shares many features of chemical reaction-diffusion dynamics. Initialization of chemotactic signals plays an important role in the initial position of aggregates [2, 7] and subsequent signaling biases cell motion towards developing aggregates [2]. Cells following the maximal chemical gradient navigate towards aggregates which are large and near. In myxobacteria, however, aggregates form without the aid of chemotactic cues [8, 9]. Yet myxobacteria travel large distances to enter an aggregate [10]. Recent cell models based on cell collisions has reproduced the myxobacteria rippling patterns that proceed aggregation, but did not attempt to model aggregation [11].

During aggregation, myxobacteria cells are elongated with a 7:1 length to width ratio (cells are typically 2 to 12 by 0.7 to 1.2 μm [12]). They move on surfaces by gliding along their long axis [13]. The stages of fruiting body development, including aggregation, are controlled by a membrane-associated signaling protein *C-factor*. Cells lacking C-factors fail to aggregate [14] while high concentrations of exogenous C-factor induce aggregation [15, 16]. Cells exchange C-factors at cell poles [16–19]. Gliding motility accounts for cell-cell alignment which is required for C-factor exchange [17, 19, 20] and subsequent C-signaling further induces alignment [21]. Aggregates range in size between 10 and 1,000 μm and are composed of 10^4 to 10^6 cells [12].

Several models have been proposed to explain myxobacteria aggregation [9]. One describes aggregation by cells following slime trails deposited by other cells, but finds these aggregates unstable without additional chemotaxis [22]. Another suggests that cells form streams by sequential end-to-end contacts due to C-signaling, which coalesce or spiral in on themselves. This model predicts that aggregates remain unstable as long as cells are motile [21]. However, experiments show cells move with faster velocities within aggregates [23].

We report a new mechanism for aggregate formation in myxobacteria: *short range interactions facilitated by streams*. This mechanism, based entirely on local cell-cell interactions, accounts for both initialization and formation of large stable aggregates in a two-stage process. First, aggregates appear in random positions and cells join aggregates by random walk. Second, the aggregates reorganize as cells redistribute by moving within transient streams connecting aggregates. We use a template-based cell model introduced in [24].

Model.— Our model is based on local rules by which cells turn preferentially in directions that increase their level of C-signaling. Cells move on a hexagonal lattice with periodic boundary conditions in all directions. Unit velocities *(or channels)* are allowed in each of the six directions. Cells are initially randomly distributed with cell density 10, where cell density is the total cell area divided by total lattice area. We model identical rod-shaped cells as 3×21 rectangles and assume a cell size of 1×7 μm. Each cell is represented as follows: (1) a single occupied lattice node corresponds to the position of the cell's center in the xy plane, (2) an occupied channel at this node designates cell's velocity, and (3) a local neighborhood defines the physical size and shape of the cell. By an exclusion rule, there may only be one cell center per channel per node. We also keep track of the C-signal exchange neighborhood of each occupied node which defines the possible locations of end-to-end overlaps between C-signaling cells. The total C-signaling neighborhood for each cell is fourteen nodes; seven at each cell pole separated by one half a cell length from the cell center. Representing a cell as an oriented point with an associated cell-shape is computationally efficient, yet approximates aggregates more closely than using point-like cells. We have also solved the cell stacking problem since overlapping cell shapes correspond to cell stacking. For example, for these 3×21 cells, up to 378 cells may stack over a node without violating the exclusion rule.

Cells first turn stochastically 60 degrees clock-wise or counter-clockwise, or stay in its current direction. Our model favors directions that maximize the overlap of the

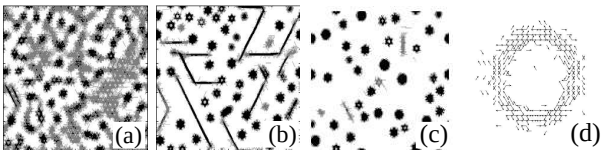

FIG. 1: Aggregation stages on a 500 × 500 lattice, which corresponds to an area of 2.8 cm^2. Local cell density after (a) 200, (b) 900, and (c) 25,000 timesteps. Average cell density is 10. The number of simulated cells is 39,507. The darker shade of gray corresponds to higher cell density. (d) Directions of cell centers within a typical annular aggregate.

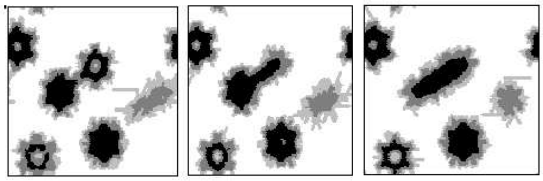

FIG. 2: The stream formation from two adjacent aggregates. Panels left to right correspond to 900, 1000, and 1200 timesteps, respectively. Lattice size is 128 × 128.

C-signal exchange neighborhood at the head of a cell with the C-signal exchange neighborhood at the tails of neighboring cells. This rule causes cells to align, which is a simplification of the hypothesis that alignment induces C-signaling which further induces cell alignment. Then, all cells move synchronously one node in the direction of their velocity by updating the positions of their centers.

Simulation Results.— Cells aggregate in distinctive stages in our simulations. During the first stage, cells turn from low density areas towards areas of slightly higher cell density. Initially randomly distributed cells condense into small stationary aggregates (Fig. 1 (a)). These aggregate centers grow and absorb immediately surrounding cells. Next, some adjacent stationary aggregates merge and form long, thin streams which extend and shrink dynamically on their own and in response to interactions with other aggregates (Fig. 1 (b)). In each stream cells move head to tail with each other in either direction along the stream. These streams are transient and eventually disappear at later stages of the simulation, leaving behind a new set of larger, denser stationary aggregates which are stable over time (Fig. 1 (c)). Cells in a typical aggregate form an annulus of aligned cells tangent to a hollow center (Fig. 1(d)).

Figure 2 shows the details of stream formation from two interacting aggregates. Initial aggregates crowd as they grow. When the distance between aggregates is less than one cell length, they begin exchanging cells, and the cells reorganize into a stream. In contrast to stationary aggregates, cells travel long distances in streams.

Role of noise.— We measure the areas and densities of every stationary aggregate which appeared over the course of two simulations. These aggregates fall within a narrow range in the area-density phase diagram shown in Fig. 3 (a), illustrating that for an aggregate of a given cell number, its area and density is prescribed within a narrow region, which we call an attractor region. We now analyze the stability of this attractor region with respect to two kinds of noise: 1) external noise, including those in the initial random distribution of cells and our perturbations to the system; 2) internal noise, which originate from the stochastic nature of the cell's turning process.

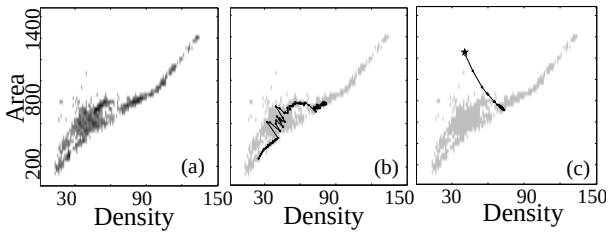

FIG. 3: Area-density phase diagram for (a) 186 stationary aggregates identified within two simulations over 25000 timesteps, (b) an initially small aggregate to which cells are slowly added over 1000 timesteps, and (c) an artificially constructed aggregate (star) over 600 timesteps. Relaxation of perturbation data in (b) and (c) are plotted every 10 timesteps on top of (a).

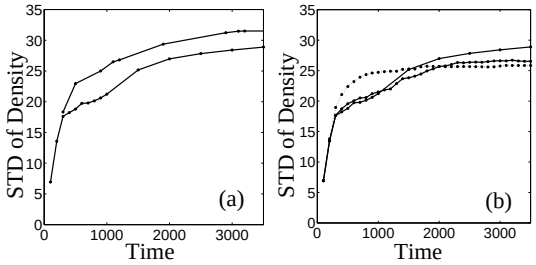

FIG. 4: Effects of external and internal noise. Standard deviation of lattice cell density over 3,500 timesteps for (a) two stochastic simulations with different initial conditions and (b) two stochastic simulations (solid lines) and one deterministic simulation (dotted line) with the same initial conditions.

1. External noise. — Figure 4 (a) shows simulation results for different random initial conditions. The standard deviation of lattice density increases with similar slope and to similar levels in the two simulations, indicating that pattern formation and simulation dynamics are not very sensitive to noise due to initial conditions.

Next we perturb a stable aggregate in two ways. First, we study an adiabatic perturbation by gradually adding cells to an initially small, isolated aggregate. As cells are slowly added, the aggregate increases in area and density while remaining within the attractor region (Fig. 3(b)). Second, we introduce a non-adiabatic perturbation by placing two duplicate aggregates in close proximity of

each other, which creates a new aggregate with double the initial area and the same density. Over 600 timesteps, this aggregate gradually reorganizes so that it has an area and density within the stable region (Fig. 3(c)). Results from both kinds of perturbations suggest that this attractor region is a stable attractor in the area-density phase space of aggregates.

This area-density phase diagram does not only prescribe the region of stable aggregates, but also helps us to understand the formation and stability of streams. When two stationary aggregates of similar size and density interact in the first stage, their area is doubled while their density remains approximately the same. Thus, the new aggregate formed lies off the attractor region. Large aggregates with high cell density and area will fuse and quickly form a new stationary aggregate as in Fig. 3 (c). Smaller fused aggregates have a longer transient stage and are likely to form streams. Due to C-signaling, the cells form end-to-end contacts which lead them to align in a stream. This stream is bi-directional, with cells flowing equally in both directions along the stream. Given the end-to-end contacts required for C-signaling, an infinitely long stream of cells flowing in two directions is obviously a stable arrangement. However, there are a fixed number of cells within simulation streams, and thus streams are of finite length. Cells at the end of streams are not stable since cells do not C-signal in the open space, hence cells at these locations will diffuse without any preferred direction. Though some cells diffuse away, most cells randomly turn within a number of timesteps back into the stream. Once cells are re-directed towards the stream, their direction is locked since they are again C-signaling with the stream cells. Cells turning back into the stream over time causes the stream to gradually contract into a stable aggregate.

2. Internal noise. — To evaluate the roles of internal noise, we devise an equivalent deterministic model. Instead of using a stochastic process to model cell turning, we use the following function to decide on the cell orientation for the next step:

$$f_i(r,k+1) = f_{i^\ominus}(r-c_{i^\ominus},k)\Omega(r-c_{i^\ominus},k,c_i)$$
$$+f_{i^\oplus}(r-c_{i^\oplus},k)\Omega(r-c_{i^\oplus},k,c_i)+f_i(r-c_i,k)\Omega(r,k,c_i)$$

where f is the particle density distribution function over each lattice node r, k is the timestep, and c_i, $c_{i^\ominus}$, and $c_{i^\oplus}$ represent velocity vectors in the ith direction, one turning clockwise from the ith direction, and one turning counter-clockwise respectively. The collision function $\Omega(r,k,i)$ is the probability of a cell at the node r turning towards direction i at the kth timestep. We drop the exclusion principle so that the density of cells may be greater than 1 at a node. This function effectively converts the stochastic process of cell turning into a continuous distribution function, analogous to the process of changing a stochastic lattice gas model to a deterministic lattice Boltzmann model [25].

Our simulations show that this deterministic model evolves similarly to the stochastic model, indicating that the aggregation dynamics are not sensitive to internal noise. Figure 4 (b) shows the standard deviation of average cell density over time for two stochastic and one deterministic simulation with identical initial conditions. As in the stochastic model, the deterministic model proceeds in stages. First many small aggregates appear, then streams form between interacting aggregates, until the streams dissolve and leave behind a larger set of aggregates. One important difference is that streams in the deterministic model are fewer and smaller. Another difference is that streams are shorter-lived, and the deterministic simulation reaches a steady state much faster. These differences have a critical effect on the way aggregates reorganize. Comparing the size distribution of aggregates in the stochastic model (Fig. 5(a)) with that of the equivalent deterministic model (Fig. 5(b)), we see that with the internal noise, aggregates can reach larger sizes. This is not surprising because noise slows the process of stream contraction so that streams persist longer and span a greater area, which enables more aggregates to interact and eventually form larger, more stable aggregates.

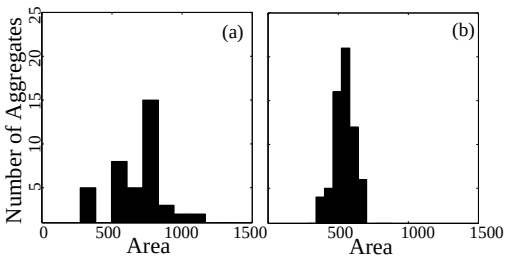

FIG. 5: Distribution of stationary aggregate areas for (a) a stochastic simulation after 29000 timesteps and (b) the equivalent deterministic simulation after 3500 timesteps. Both distributions represent the final stable distribution.

Discussion.— In our simulations, streams redistribute cells within fewer, larger aggregates (compare Fig. 1 (a) and (c)). This is a new mechanism for large, stable aggregate formation in which aggregates form at random and then redistribute. The mechanism is robust since streams form when growing aggregates develop too close together. Cells can then span great distances by moving within streams. Streams resettle into stationary aggregates by moving into a pre-existing stationary aggregate or by gradually thickening and contracting.

The aggregates in our simulation reproduce the unique structures of several myxobacteria fruiting bodies. In *Myxococcus xanthus*, the basal region of the fruiting body is a shell of densely packed cells which orbit both clockwise and counter-clockwise around an inner region only one-third as dense [23, 26]. A magnified picture of the cell centers of a typical aggregate in our simulation show that cells are arranged in a dense, concentric layer tangent to a relatively low-density inner region (Fig. 1 (d)) and cell tracking shows that cells orbit either clockwise or anti-clockwise along the periphery of the orbit. Further,

aggregates in our simulation often form in clusters of two or three closed orbits while in *Stigmatella erecta*, several fruiting bodies may form in groups and fuse [12].

In experiments, one myxobacteria aggregate has been observed to mysteriously grow as an adjacent aggregate disappears [27]. Our simulations offer a mechanism for this process: a stream may form connecting two adjacent aggregates and, following a C-signaling line of cells, cells stream from the smaller aggregate to the larger aggregate. Experimentally, these streams may not be visible if the density threshold for viewing cells is greater than the density found within the stream.

This mechanism suggests several predictions which may be tested experimentally. We predict that the formation of streams and subsequent redistribution of aggregates will be most significant for intermediate initial cell densities. At low density, the initial set of aggregates will form further apart and will not grow as large. At high cell density, very large, dense aggregates form, which fuse immediately into a larger aggregate when they interact rather than forming a stream. The role of external noise can be experimentally tested by reproducing the perturbation experiments we describe in Figure 3(b) and 3(c). Cells may be slowly added to a small aggregate or quickly added to an aggregate by a large amount to observe the cell reorganization over time. Finally, the role of internal noise can be tested experimentally by tuning the amount of C-factor in the cell aggregates. For example, C-signaling can be decreased by diluting a wild-type population with non-C-signaling cells (increasing internal noise) or individual cell C-signaling levels can be increased (decreasing internal noise).

Summary.— Our lattice cell model is based on a very simple local rule in which cells align by turning preferentially to make end to end contacts. This mimics C-signaling in myxobacteria, which drives myxobacteria aggregation. Myxobacteria cells behave in a collective way without losing their identity as individual cells. In our simulations, distinct aggregate types form which have different behaviors and roles even though they are composed of identical cells following identical rules. Large, stationary aggregates are most stable, but an intermediate motile aggregate forms which aids in large aggregate formation. An interesting discovery is that the presence of some internal noise is required for efficient streaming. It is as if the cells must make short-term mistakes for the formation of unstable transients that ultimately results in more efficient aggregation. Our analyses of streams and the role of noise suggest some new experiments.

We thank Drs. Dale Kaiser, Stan Maree and Guy McNamara for fruitful discussions. MSA is partially supported by grant NSF IBN-0083653. MAK and YJ are supported by DOE under contract W-7405-ENG-36. MAK also acknowledges support from CAM and ICSB centers, University of Notre Dame.

[1] E. Ben-Jacob *et al.*, Nature (London) **368**, 46 (1994).
[2] L. Tsimring *et al.*, Phys. Rev. Lett. **75**, 1859 (1995).
[3] M. P. Brenner, L. S. Levitov, and E. O. Budrene, Biophys. J. **74**, 1677 (1998).
[4] M. Matsushita and H. Fujikawa, Physica A **168** 498 (1990); I. Golding, Y. Kozlovsky, I. Cohen, and E. Ben-Jacob, Physica A **260**, 510 (1998); A. Komoto *et al.*, J. Theor. Biol. **225**, 91 (2003).
[5] E. Ben-Jacob, I. Cohen, and H. Levine, Adv. Phys. **49** 4, 395 (2000).
[6] J. Martiel and A. Goldbeter, Biophys. J. **52**, 807 (1987); T. H ofer, J.A. Sherratt, and P.K. Maini, Proc. R. Soc. London B **259**, 249 (1995).
[7] J.Y. Wakano *et al.*, Phys. Rev. Lett. **90**, 258102 (2003).
[8] S. Lobedanz and L. Søgaard-Andersen, Genes Dev. **17**, 2151 (2003).
[9] For a review see M. Dworkin, Microbiol. Rev. **60**, 70 (1996).
[10] L. Jelsbak and L. Søgaard-Andersen, Curr. Opinion Microbio. **3**, 637 (2000).
[11] O. Igoshin, A. Mogilner, D. Kaiser, and G. Oster, Proc. Natl. Acad. Sci. USA **98**, 14913 (2001); U. Borner, A. Deutsch, H. Reichenbach, and M. Bar, Phys. Rev. Lett. **89**, 078101 (2002).
[12] H. Reichenbach, in: M. Dworkin and D. Kaiser (Eds), *Myxobacteria II*, (American Soc. Microbio., Washington DC, 1993).
[13] R.P. Buchard, Annu. Rev. Microbiol. **35**, 497 (1981).
[14] D. Hagen, A. Bretscher, and D. Kaiser, Dev. Bio. **64**, 284 (1978).
[15] L.J. Shimkets, R.E. Gill and D. Kaiser Proc. Natl. Acad. Sci. USA **80**, 1406 (1983); S.K. Kim and D. Kaiser, J. Bacteriol. **173**, 1722 (1991); S. Li, B. Lee and L.J. Shimkets, Genes Dev. **6**, 401 (1992).
[16] S.K. Kim and D. Kaiser, Genes Devel. **4**, 896 (1990).
[17] S.K. Kim and D. Kaiser, Science **249**, 926 (1990).
[18] L. Kroos, P. Hartzell, K. Stephens and D. Kaiser, Genes Devel. **2**, 1677 (1988); B. Sager and D. Kaiser, Genes Dev. **8**, 2793 (1994).
[19] S. K. Kim and D. Kaiser, Cell **61**, 19 (1990).
[20] R.P. Buchard, in: E. Rosenburg (Ed), *Myxobacteria*, (Springer-Verlag, New York, 1984); S.K. Kim and D. Kaiser, Proc. Natl. Acad. Sci. USA **87**, 3635 (1990); C. Wolgemuth and E. Hoiczyk, Curr. Bio. **12** 369 (2002).
[21] L. Jelsbak and L. Søgaard-Andersen, Proc. Natl. Acad. Sci. USA **99**, 2032 (2002).
[22] A. Stevens, SIAM J. Appl. Math. **61**, 172 (2000).
[23] B. Sager and D. Kaiser, Proc. Natl. Acad. Sci. USA **90**, 3690 (1993).
[24] M. S. Alber, Y. Jiang, and M. A. Kiskowski, Physica D (to be published).
[25] U. Frisch et al., Complex Systems **1**, 648 (1987).
[26] B. Julien, D. Kaiser and A. Garza, Proc. Natl. Acad. Sci. USA **97**, 369 (2000).
[27] D. Kaiser (private communication).